Hindawi
International Journal of Aerospace Engineering
Volume 2019, Article ID 3750451, 10 pages
https://doi.org/10.1155/2019/3750451

Research Article

A Novel Aerodynamic Noise Reduction Method Based on Improving Spanwise Blade Shape for Electric Propeller Aircraft

Yuhang Wu,[1] **Yan-ting Ai**,[2] **Wang Ze**,[3] **Tian Jing**,[2] **Xiang Song**,[4] **and Yingtao Chen**[2]

[1]*School of Aerospace Engineering, Shenyang Aerospace University, Shenyang 110136, China*
[2]*Liaoning Key Laboratory of Advanced Measurement and Test Technology for Aviation Propulsion System, Shenyang Aerospace University, Shenyang 110136, China*
[3]*Geely Automobile Holdings Ltd., Hangzhou 310000, China*
[4]*Liaoning Key Laboratory of General Aviation, Shenyang 110136, China*

Correspondence should be addressed to Yingtao Chen; chenyingtao75@163.com

Received 27 September 2019; Revised 12 November 2019; Accepted 14 November 2019; Published 12 December 2019

Academic Editor: Giacomo V. Iungo

Aiming at the problem of excessive propeller noise in a new type of electric aircraft, in order to ensure the propeller aerodynamic characteristics simultaneously, a noise reduction method for improving the shape of the blade along the spanwise is proposed. The FW-H model, the unsteady slip mesh, and the large eddy simulation method are investigated to obtain the aerodynamic noise spectrum. Initially, through propeller aerodynamic noise numerical simulation, we obtain the sound pressure and aircraft aerodynamic noise in frequency domain. Subsequently, the effectiveness of our method is verified by comparing the experimental data and numerical results. Based on the established calculation model and method, under three different rotation speeds, the distribution law of the sound pressure level of the propeller with different shapes along the spanwise is analyzed, and the influence of the blade shape on the aerodynamic noise of the propeller is obtained. The research shows that the aerodynamic noise of the new blade compared to the original blade is significantly reduced at the same rotation speed higher than 1000 rpm, indicating that the blade load noise plays a dominant role in the aerodynamic noise and can be effectively reduced by changing the blade shape along the spanwise, thus reducing the aerodynamic noise of the blade.

1. Introduction

The propellers, as devices converting rotational power of aeroengines into propulsion, result in aerodynamic noise for airplanes. Due to such noise, uncomfortable feelings for passengers, bad airport environment, flight safety threats, and so on are caused in practice. Propeller noise belongs to the category of aeroacoustics and is caused by unsteady flow field pulsations which is caused by high-speed rotation of the propeller. Current noise reduction methods include reducing the intensity of the sound source and reducing noise based on the interference of destructive sound waves. In this paper, the propeller aerodynamic noise is reduced by the intensity of the sound source through improving the propeller design. It should research the noise sounding mechanism, propeller model design, and numerical calculation of aerodynamic noise. By collecting the relevant physical quantities, analyzing the propeller aerodynamic noise and continuously improving the geometric parameters of the propeller model are to achieve the purpose of noise reduction.

Recently, many related works have been conducted on noise reduction of propeller aircraft. The influence of main design parameters for light aircraft on propeller aerodynamic noise is performed by Chusseau et al. [1], Gur and Gur and Rosen [2, 3], etc. They all achieved good prediction results but do not research on the physical quantities which affect aerodynamic noise. Antonio et al. [4], Marinus and Roger [5], and Campos and Lau [6] have complimented the multi-objective optimization design of propeller aerodynamic noise. But they did not finish the application of blade noise reduction optimization and performance analysis of the blade after noise reduction. Pan and Qian [7] proposed a numerical optimization method for propeller aerodynamic design and used the method to redesign two propellers. On

Table 1: Parameters of propeller.

Propeller diameter	1.6 m
Number of paddle blades	2
Airfoil	Clark-Y
Paddle width	88.7 mm
Pitch	1.25 m
Hub radius	0.06 m
Hub height	0.06 m

the basis of Lighthill and Curle's basic research, Bazhenova [8] used an improved method to measure the pressure pulsation of rotating blades and stationary components of the body and revealed that the aerodynamic noise source is composed of discrete and broadband components. The above researchers have revealed the cause of propeller noise and the characteristics of the associated noise. Jiang et al. [9] used computational aeroacoustics (CAA) to obtain the unified solution of fluid-sound according to the theoretical model by solving n-s equation and studied the process of sound source, sound propagation, and acoustic radiation. Greschner et al. [10] calculated the flow field and sound field separately. Firstly, flow field information was obtained through CFD calculation, and the frequency domain distribution of the sound source was obtained through discrete Fourier transform (DFT). Rogowski et al. [11] study the scale adaptive simulation (SAS) approach for performance analysis of a one-bladed Darrieus wind turbine working at a tip speed ratio of 5 and at a blade Reynolds number of 40000. The level of agreement between CFD and experimental results is reasonable. Then, propeller noise characteristics were calculated by the acoustic method. Wisniewski et al. [12] explored the influence on performance and noise by changing the geometric parameters of propeller wings. However, the application of blade noise reduction optimization and the performance analysis of the blade after noise reduction are not performed.

In this paper, the aerodynamic noise characteristics for numerical simulation and experiment are studied, respectively. To effectively investigate the aerodynamic noise reduction method, the flow field-sound field combination calculation method is applied for numerical simulation. The propeller flow field information is obtained by CFD, and it is imported into Virtual.Lab to realize the noise characteristic analysis. In the flow field calculation process, the grid is divided by ICEM and uses the sliding mesh method for connection. A novel model is established based on the FW-H [13] method. Then, propeller aerodynamic noise characteristics are analyzed through the large eddy simulation method. In the sound field calculation, the aerodynamic noise is equivalent to the fan sound source to calculate by the direct boundary element (BEM) method in Virtual.Lab, and the distribution law of the aerodynamic noise pressure level of the propeller at five different speeds is obtained. Meanwhile, to obtain sound pressure overall intensity maps, as well as the aerodynamic noise in the frequency domain, the ground far-field noise experiment under five speeds is employed based on LMS Test.Lab. Ultimately, we found that the total sound pressure level approaches low-order BPF (blade pass frequency). With modifying the shape of the blade along the spanwise, the load noise can be effectively reduced, and the noise reduction optimization of the propeller aerodynamic noise is completed. The wind tunnel test of the scale reduction model proves that the new propeller blade has good aerodynamic performance after noise reduction optimization, meeting the flight standards.

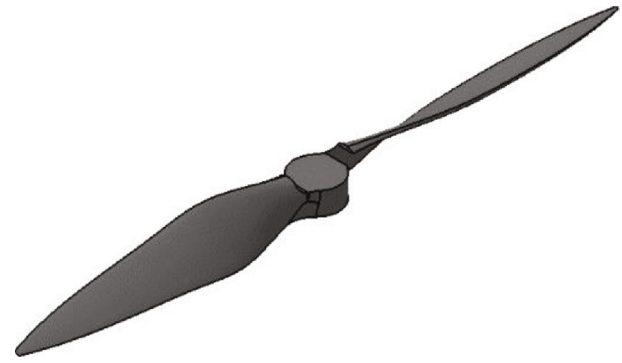

Figure 1: Propeller model.

2. Aerodynamic Noise Numerical Simulation

2.1. Geometric Modeling and Grid Divided. According to the method proposed by Angelo et al. [14] and the low-noise propeller design theory presented by Xiang et al. [15], the maximum efficiency propeller under a given working condition is designed. According to the parameters in Table 1 such as propeller diameter, pitch, number of blades, hub radius, and height and Clark-Y airfoil data shown, we utilize Catia software to generate leaf foliar.

Then, a three-dimensional model of the propeller is established, as depicted in Figure 1. The superiority of this method is avoiding too many points and curves resulting from change of coordinates in obtaining the blade section, which reduces the workload and improves the fault tolerance rate. We divide the grids in ICEM into two parts: the inner field rotation domain and the outer field static domain. The structured tetrahedral mesh is used in the inner rotation field, while unstructured hexahedral mesh is used in the outer rest area. As shown in Figure 2, these two parts are processed by a sliding patch, and the total number of grids is approximately 3.87 million. The boundary layer grid around the blade is shown in Figure 3.

2.2. Parameter Setting and Blade Pressure Pulsation Solution. The inlet area interface is set as the pressure inlet, while the outlet one is the pressure outlet. Additionally, the rotation area is set as an interface, the rotation area fluid type is set to fluid, and the rest of the propeller profile boundary type is set as the wall.

To obtain the turbulent flow field characteristics of the propeller, unsteady calculation is utilized in our work. The most compliant large eddy simulation (LES) model is employed to derive pressure discrete format by PRESTO under the rotating speeds of 500 rpm, 1000 rpm, 1500 rpm, 2000 rpm, and 2200 rpm, respectively. As aforementioned, the mass flow rate curve of blade tends to converge under

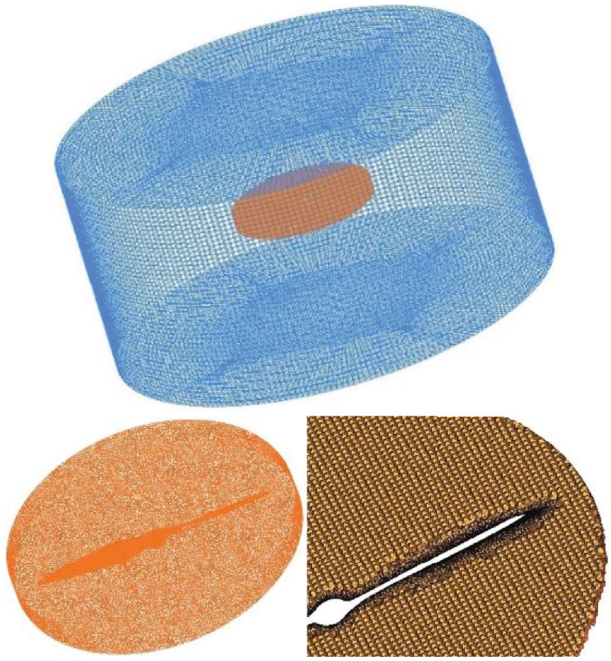

Figure 2: Global grid division.

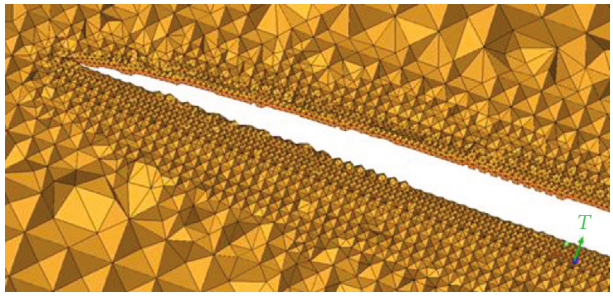

Figure 3: Boundary layer grid around the blade.

20 disturbance periods. Thus, the number of iterative steps is set as 1500 steps. According to the formula Time size = $20T/1500$, the time steps at each speed are $\Delta t_1 = 8 \times 10^{-4}$ s, $\Delta t_2 = 4 \times 10^{-4}$ s, $\Delta t_3 = 2.7 \times 10^{-4}$ s, $\Delta t_4 = 2 \times 10^{-4}$ s, and $\Delta t_5 = 1.8 \times 10^{-4}$ s, respectively. In the Fluent calculation, the exit flow monitoring curve and the area weighted average curve tend to be stable, and the residual converges to 10^{-4}, which is considered to be a steady state. In the following part, the files generated in Fluent is imported into Virtual.Lab and the noise analysis will be carried out.

2.3. Spherical Model Establishing to Analyze Propeller Aerodynamic Noise. In order to obtain noise characteristics of the propeller in the far-field area, a sphere with origin of propeller center and a radius of 15R (24 m, the same distance from aerodynamic noise experiment) is created, where the material property is air, as shown in Figure 4.

After defining the properties of fluid and propeller source, the operation is submitted. The noise data processed by large eddy simulation and FW-H model are subjected to fast Fourier transform (FFT) to obtain the sound pressure level of the aerodynamic noise of the propeller. The noise

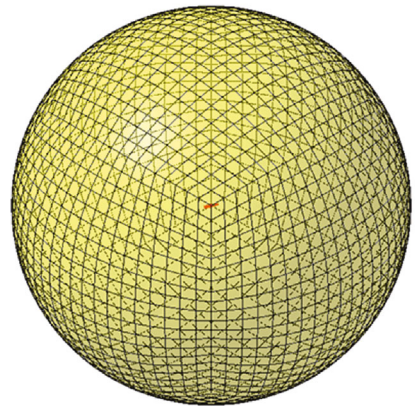

Figure 4: Spherical acoustic radiation model.

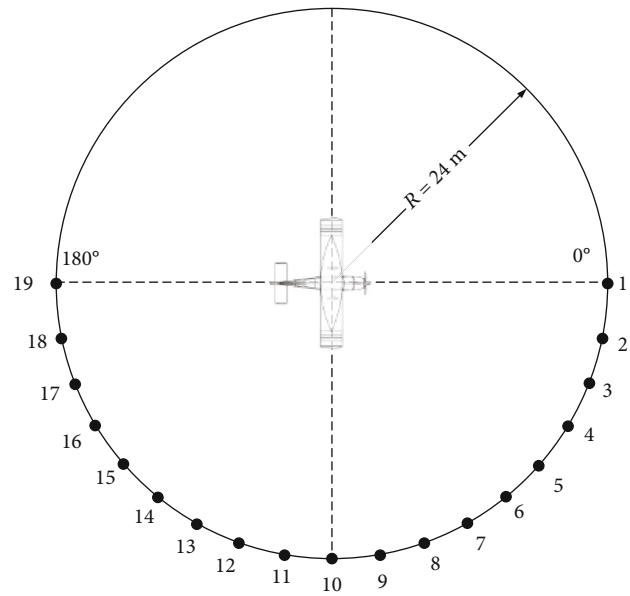

Figure 5: Noise receiver position schematic diagram.

receiver position schematic diagram is defined in Figure 5. The results show that the aerodynamic noise and other sound pressure lines are distributed along the axial strip. Moreover, the points with higher sound pressure appear on the upper and lower surfaces of the ball, as well as both ends of the axial direction, while the sound pressure in one radial direction is lower. Specifically, when the rotating speeds are 500 rpm, 1000 rpm, 1500 rpm, 2000 rpm, and 2200 rpm, the corresponding maximum sound pressure of spherical field radiations are 40.1 dB, 62.2 dB, 70.1 dB, 80.1 dB, and 85.9 dB, respectively. Because the numerical simulation does not add ground reflection, the calculated value is 6 dB less than the experimental value, which is consistent with Yin and Hu's conclusion [16]: the correction amount of the sound field free-field sound pressure level considering the ground reflection is 6 dB. Therefore, the calculated value is corrected.

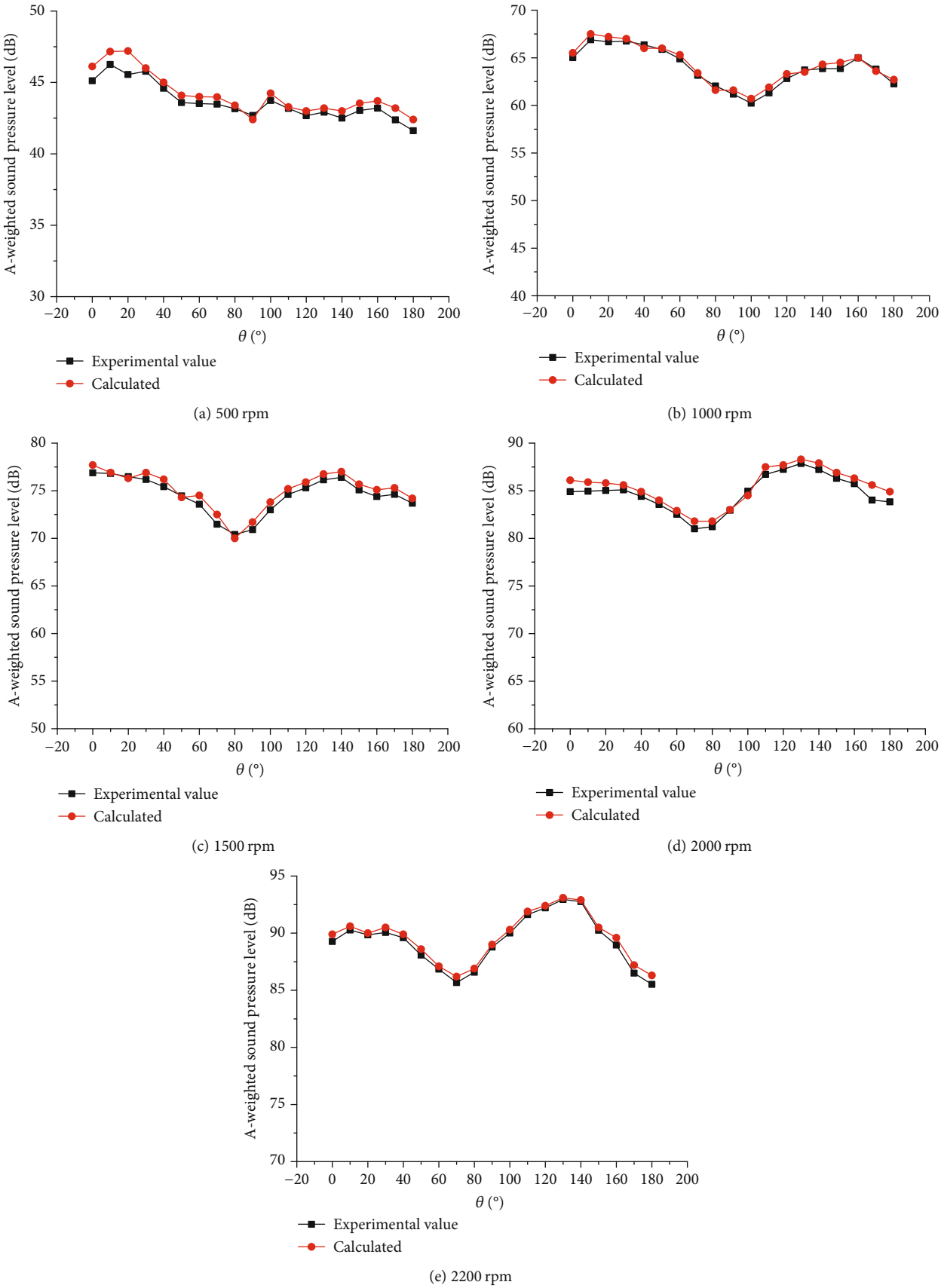

Figure 6: Noise pressure level distribution under each rotating speed.

Figure 7: The experimental site.

Figure 8: Propeller plan.

Meanwhile, the maximum sound pressures at five rotation speeds all occur near ends of the spherical field point in the axial direction. The effectiveness of the proposed method is verified by the experimental and calculated values of aerodynamic noise, as presented in Figure 6.

3. Ground Far-Field Noise Test

To obtain far-field aerodynamic noise data, the complete ground noise test of the propeller was implemented according to the standard SAE ARP 1846A [17]. To ensure that the experiment is not affected by other factors, an open space without any buildings or other obstructions within a radius of 500 m of the aircraft was selected. The layout of the site and the propeller aircraft are shown in Figures 7 and 8, respectively.

The arrangement of noise measurement points is shown in Figure 5. Such measurement points are arranged at every 10° on the circumference with the radius 24 m. We set the forward axis of the propeller as the no. 1 measuring point, and the total measurement points are 19.

Through the frequency formula $f = Bn/60$, we obtain the BPF as 16.7 Hz, 33.3 Hz, 50 Hz, 66.7 Hz, and 73.3 Hz, respectively. Those results approach to the measured baseband signal frequency, as shown in Figure 9. In Figure 9, the horizontal axis represents frequency, in Hz. The vertical axis represents the sound pressure level at the measurement point, in dB. Obviously, propeller far-field aerodynamic noise is composed of continuous broadband noise and a series of discrete noises. These discrete noises, including fundamental frequency and frequency multiplication signals, have periodic characteristics. Compared with broadband noise, the sound pressure levels of discrete noise are mainly distributed around the low-order BPFs. With the increase of the rotational speed, the discrete noise spectrum is more clearly separated and the frequency multiplication signal is more prominent especially in the 1500 rpm, 2000 rpm, and 2200 rpm speed spectrum charts. It is similar to the total sound pressure level of aerodynamic noise. The results verify that discrete noise is the main factor for propeller aerodynamic noise when rotating speed increases. These discrete noises are induced by the interaction between the propeller and air in the periodic cutting flow field. The total sound pressure level of propeller aerodynamic noise at no. 10 measuring point with different speeds is shown in Table 2.

Figure 10 presents the distribution of sound pressure level test results with five different speeds. Clearly, far-field aerodynamic noise increases with the adding rotating speed. The distributions of circular field points at different rotational speeds are roughly the same, which means that the increasing rotational speed cannot change the directivity of the aerodynamic noise. When the rotation speed is 500 rpm, the noise change in the circumferential direction is not obvious, as shown in the 10th and 19th test point. When the rotation speed increases from 500 rpm to 1000 rpm, the noise growth is most obvious. For the rotational speed from 1000 rpm to 1500 rpm, the noise change is relatively minimal. The noise variation for the rotational speed from 1500 rpm to 2200 rpm is smaller than that from 1000 rpm to 1500 rpm. It illustrates that the rotating speed mainly determined the propeller aerodynamic noise when such speed is less than 1000 rpm. When the rotating speed is larger than 1000 rpm, the variation of aerodynamic noise is gradually decreased with the increase of rotating speed.

4. Noise Reduction Simulation Contrast

Aerodynamic noise of the propeller includes broadband noise and rotational noise. Broadband noise is induced by the interaction between the propeller and air in the flow field, while rotational noise is caused by periodically cutting air of the propeller in the flow field.

Generally, the random aerodynamic components of rotating blades resulting in the propeller broadband noise is induced by several factors, such as rogue flow, random vorticity from the trailing edge of the blade, and the turbulent boundary layer of the paddle [18, 19]. Therefore, the quantitative estimation of broadband noise is still difficult. Moreover, the broadband noise is much smaller than the rotational noise, when the propeller operates in the steady state.

According to noise characteristics, the rotational noise can be divided into three parts: blade thickness noise, load noise, and quadrupole noise [20]. Blade thickness noise [21, 22] is induced by the unsteady movement of air micelles

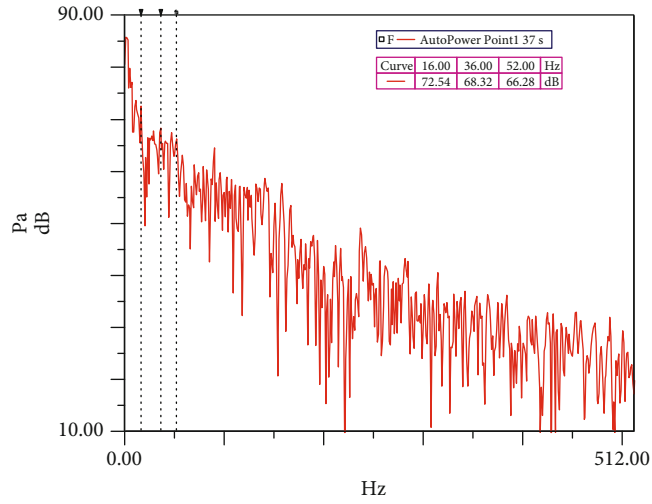

(a) 500 rpm noise spectrum

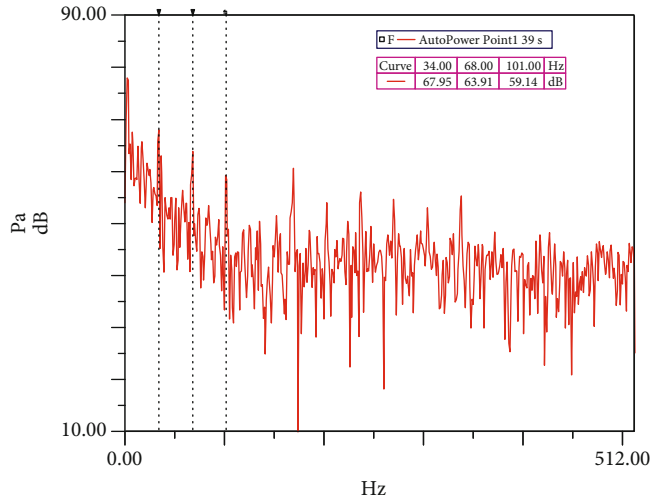

(b) 1000 rpm noise spectrum

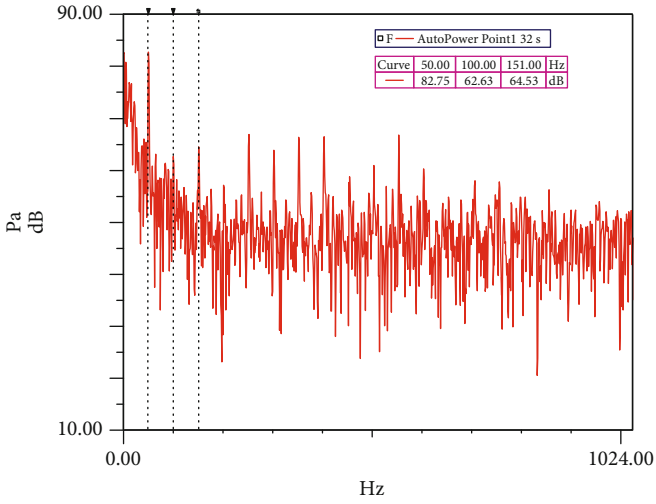

(c) 1500 rpm noise spectrum

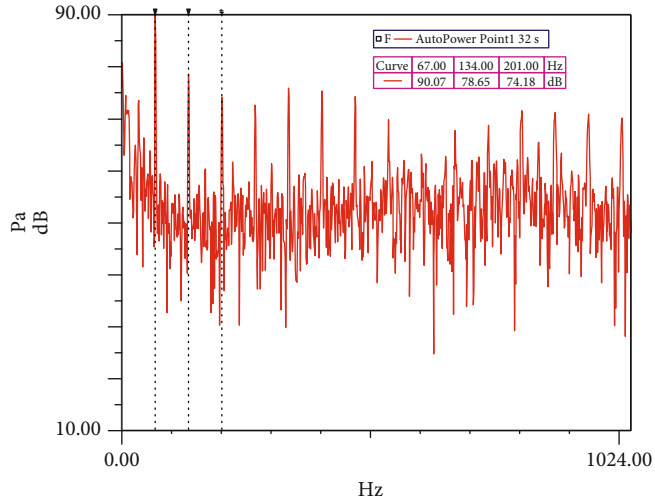

(d) 2000 rpm noise spectrum

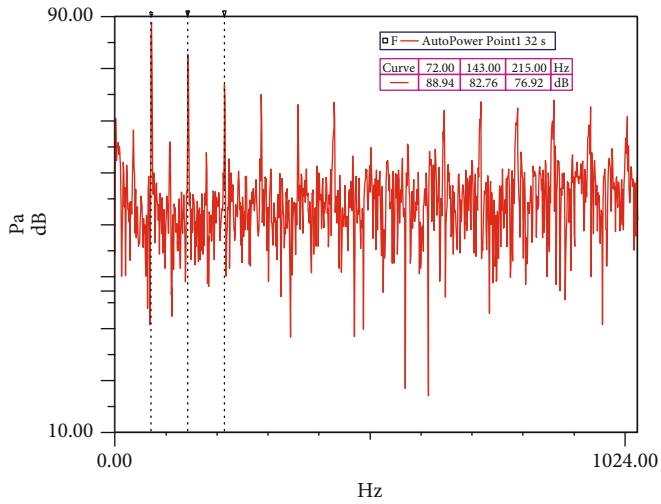

(e) 2200 rpm noise spectrum

Figure 9: Noise spectrum in different speeds.

Table 2: Total sound pressure level of propeller at no. 10 measuring point of propeller (A).

n (rpm)	Experimental value (dB)
500	56.97
1000	72.39
1500	84.65
2000	91.3
2200	91.87

when the blade periodically sweeps around the surrounding air medium. Load noise, considered as the combination of tension noise and resistance noise, is caused by the pressure field of the rotating blade when the engine drives the propeller and generates tension and resistance. Both thickness noise and load noise show periodical laws. Propeller quadrupole noise is determined by two key factors: nonlinear source and nonlinear propagation. The noise source is only considered when the propeller tip is working in supersonic and transonic operating conditions. Since our paper only considers the pneumatic noise of propeller aircraft flying at subsonic speed, the quadrupole noise can be ignored. Obviously, the aerodynamic noise of the propeller can be expressed by the propeller thickness noise and load noise [23, 24].

This paper focuses on the intensity of the sound source to reduce the noise of the propeller aerodynamic noise. By improving the shape along the spanwise of the blade and increasing the width of the blade in the radial direction, the propeller load noise is reduced, because the tip of the blade is the highest in terms of radial distribution of noise sound power. Then, we optimize the width of the blade in the radial direction to reach the noise reduction limit. Finally, we obtain the improved blade with the geometric parameters shown in Table 3. Compared with the original blade, the width increment of the improved blade paddle is 59.7 mm.

According to the same numerical simulation of aerodynamic noise, the far-field aerodynamic noise of the improved blade is calculated at the speed of 1000 rpm, 1500 rpm, and 2000 rpm. The spherical pressure point sound pressure cloud diagram at different rotational speeds is shown in Figures 11, 12, and 13. The maximum noise is distributed on the front and rear sides of the paddle shaft. The aerodynamic noise distribution on the plane of the paddle axis has a similar shape of "8," which is a typical load noise characteristic. Contrast same speed spherical field sound pressure cloud, the low-noise area in the rotating plane of the propeller gradually becomes smaller, and the noise band distributed in the axial direction tends to be moderated at the same time. It shows that the load noise accounts for a lower proportion of the aerodynamic noise. Comparing Figures 11(a), 12(a), and 13(a), the adding rotation speed increases the aerodynamic noise, but it does not change the radiation directivity of the noise.

Table 4 lists the far-field aerodynamic noise experimental data and the aerodynamic noise data obtained under different blade widths. As can be seen, the original blade calculated

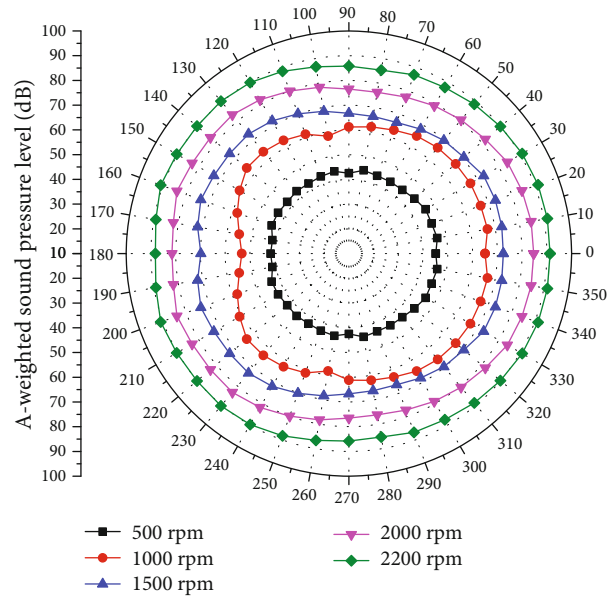

Figure 10: Total acoustic pressure level of the measurement point (A).

Table 3: New propeller geometry.

Propeller diameter	1.6 m
Number of paddle blades	2
Airfoil	Clark-Y
Paddle width	148.4 mm
Pitch	1.25 m
Hub radius	0.06 m
Hub height	0.06 m

results are smaller than the experimental ones. The error between experimental data and the original blade calculated data approaches to 2.2 dB at 1000 rpm, 1.7 dB at 1500 rpm, and 0.8 dB at 2000 rpm. The maximum noise reduction of the improved blade, compared to the original blade, is 11.4 dB at 1000 rpm, 9.2 dB at 1500 rpm, and 8.3 dB at 2000 rpm. Clearly, the improved blades suppress the aerodynamic noise significantly.

To verify the aerodynamic performance of the new blade, the propeller model was made at a ratio of 1 : 0.6 with the full wooden materials. Meanwhile, such model passed the proportional propeller test in a wind tunnel, as shown in Figure 14.

The proportional propeller test is implemented in the wind tunnel with the cruising wind speed 30 m/s. The derived propeller performance data is shown in Table 5, where n represents rotating speed, λ is forward ratio, C_r is pull coefficient, C_q denotes torque coefficient, C_w is power factor, and η represents efficiency. It can be seen that the pull coefficient, torque coefficient, and power coefficient decrease as the forward ratio increases. When the forward ratio reaches 0.637~0.799, the efficiency of the propeller reaches more than 80%, which meets the flight aerodynamic performance requirements.

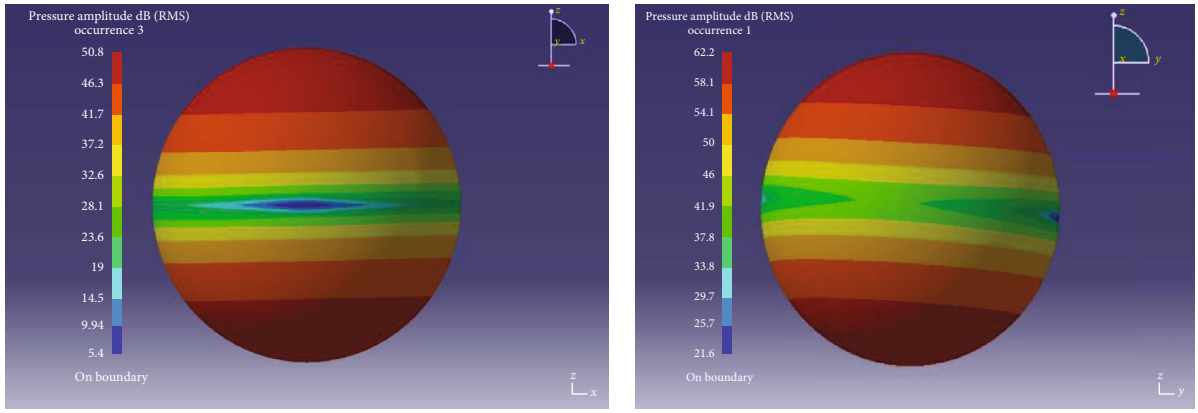

(a) New blade (b) Original blade

Figure 11: 1000 rpm spherical field sound pressure cloud.

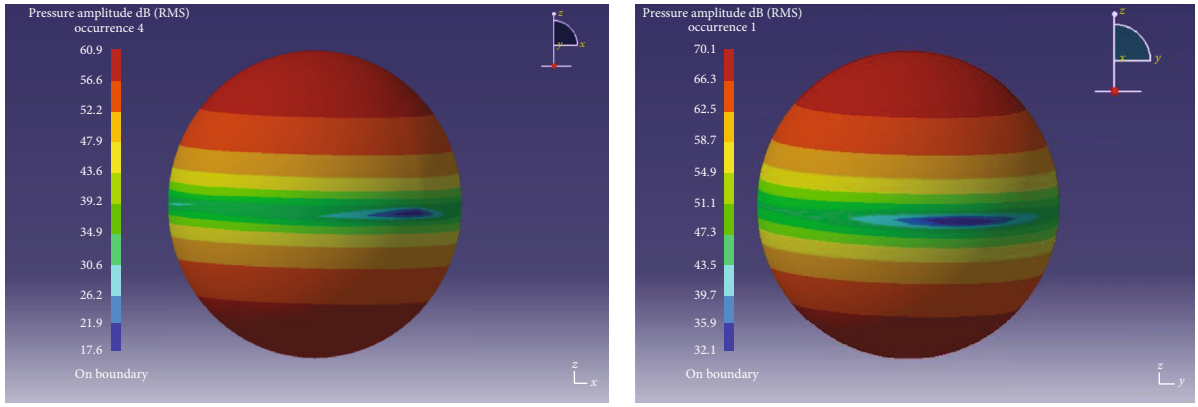

(a) New blade (b) Original blade

Figure 12: 1500 rpm spherical field sound pressure cloud.

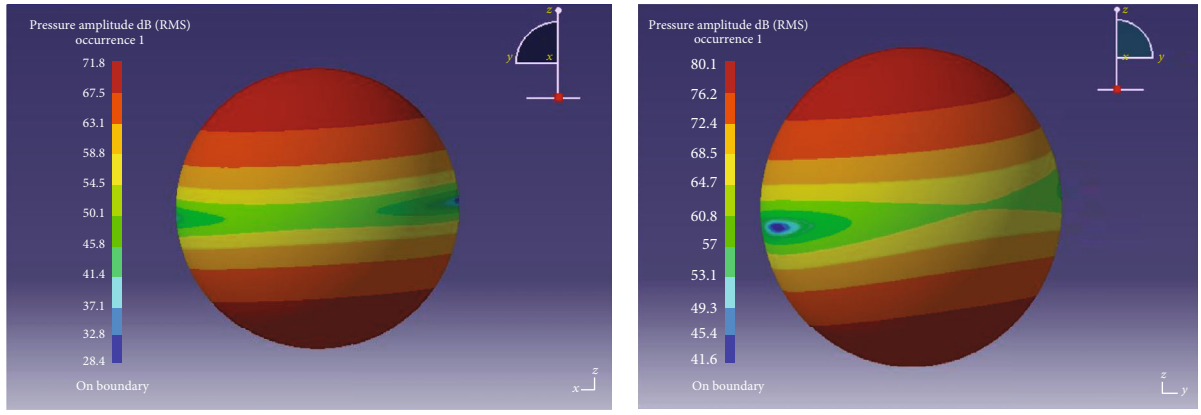

(a) New blade (b) Original blade

Figure 13: 2000 rpm spherical field sound pressure cloud.

5. Conclusion

This paper mainly studies the noise reduction of an electric propeller aircraft. Initially, aerodynamic noises for blades with different shapes along the spanwise are calculated. Sound pressure level laws and distribution of aerodynamic noise were analyzed. Then, a ground far-field noise experiment and wind tunnel experiment are implemented. Through the experiments, three major findings can be obtained:

(1) The rotating speed affects the aerodynamic noise in different speed ranges. For the rotating speed less than 1000 rpm, the aerodynamic noise increases

Table 4: The sound pressure value of the propeller at corresponding speed.

n (rpm)	Experimental value (dB)	Original blade (dB)	New blade (dB)
1000	66.0	68.2	56.8
1500	77.8	76.1	66.9
2000	86.9	86.1	77.8

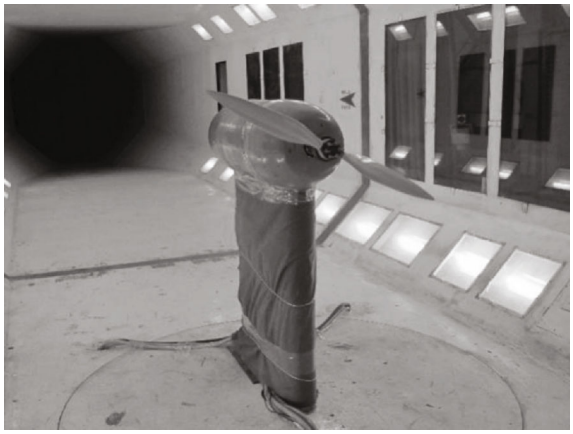

Figure 14: Propeller in the wind tunnel.

Table 5: Propeller performance data (wind speed 30 m/s).

n (rpm)	λ	C_r	C_q	C_w	η
2100	0.916	0.023	0.0045	0.028	0.755
2400	0.799	0.045	0.0065	0.041	0.868
2700	0.709	0.059	0.0077	0.048	0.867
3000	0.637	0.070	0.0084	0.053	0.841
3300	0.579	0.077	0.0089	0.056	0.798

greatly as the rotating speed increases. For the rotating speed larger than 1000 rpm, aerodynamic noise is mainly determined by discrete noise. Furthermore, the increasing rotating speed cannot change in the directivity of aerodynamic noise

(2) Propagating pressure lines of the propeller in the spherical sound field are distributed along the axial sides. The maximum noise is distributed on the front and rear ends of the paddle in the axial direction. The numerical simulation of sound pressure level distribution is consistent with the experimental values, verifying the correctness of the calculation

(3) The improved blades suppress the aerodynamic noise significantly while meeting flight standards. It is feasible to reduce the propeller aerodynamic noise by changing the blade shape along the spanwise

Data Availability

All data used to support the findings of this study are included within the article.

Conflicts of Interest

The authors declare that they have no conflicts of interest.

Authors' Contributions

Research approach and program proposed by Yingtao Chen and Yanting Ai. Research funding by Yingtao Chen. Literature studied by Yuhang Wu, Jing Tian and Yanting Ai. Experiment and data collection investigated by Yuhang Wu, Ze Wang and Xiang Song. Data analysis, and results analysis and discussion finished by Yuhang Wu and Ze Wang. Paper written by Yuhang Wu and Yingtao Chen.

Acknowledgments

The authors would like to acknowledge the support by the National Natural Science Foundation of China (Grant No. 11302133) and Liaoning Key Laboratory of General Aviation.

References

[1] M. Chusseau, E. Roozen, S. Pauzin, P. Matharan, and A. Carrère, "Light aircraft propeller - design parameter effects on acoustics and aerodynamics," in *15th Aeroacoustics Conference*, Long Beach, CA, U.S.A, October 1993.

[2] O. Gur, "Maximum propeller efficiency estimation," *Journal of Aircraft*, vol. 51, no. 6, pp. 2035–2038, 2014.

[3] O. Gur and A. Rosen, "Optimization of propeller based propulsion system," *Journal of Aircraft*, vol. 46, no. 1, pp. 95–106, 2009.

[4] A. Pagano, L. Federico, M. Barbarino, F. Guida, and M. Aversano, "Multi-objective aeroacoustic optimization of an aircraft propeller," in *12th AIAA/ISSMO Multidisciplinary Analysis and Opti-mization Conference*, pp. 2008–6059, Victoria, British Columbia, Canada, 2008.

[5] B. Marinus, M. Roger, R. Van den Braembussche, and W. Bosschaerts, "Multidisciplinary optimization of propeller blades: focus on the aeroacoustic results," in *17th AIAA/CEAS Aeroacoustics Conference (32nd AIAA Aeroacoustics Conference)*, pp. 2011–2801, Portland, Oregon, 2011.

[6] L. Campos and F. Lau, "On propeller acoustics design synthesis using source distributions along blade span," in *12th AIAA/CEAS Aero-acoustics Conference (27th AIAA Aeroacoustics Conference)*, pp. 2006–2605, Cambridge, Massachusetts, 2006.

[7] J. Y. Pan and H. D. Qian, "Numerical optimization design of propeller," *Journal of Aerospace Power*, vol. 6, no. 4, pp. 300–304, 1991.

[8] L. A. Bazhenova, "Noise sources of aerodynamic origin in air Blowers," *Acoustical Physics*, vol. 64, no. 3, pp. 356–364, 2018.

[9] J. I. A. N. G. Min, L. I. Xiao-dong, and L. I. N. Da-kai, "Numerical simulation on the airfoil self-noise at low Mach number flows," in *50th AIAA Aerospace Sciences Meeting including the New Horizons Forum and Aerospace Exposition*, pp. 1492–1512, Nashville, Tennessee, 2012.

[10] B. Greschner, F. Thiele, M. C. Jacob, and D. Casalino, "Prediction of sound generated by a rod–airfoil configuration using EASM DES and the generalised Lighthill/FW-H analogy," *Computers & Fluids*, vol. 37, no. 4, pp. 402–413, 2008.

[11] K. Rogowski, M. O. L. Hansen, R. Maroński, and P. Lichota, "Scale adaptive simulation model for the Darrieus wind turbine," *Journal of Physics: Conference Series*, vol. 753, article 022050, 2016.

[12] C. F. Wisniewski, A. R. Byerley, W. Heiser, K. W. Van Treuren, and T. Liller, "The influence of airfoil shape, Reynolds number and chord length on small propeller performance and noise," in *33rd AIAA Applied Aerodynamics Conference*, pp. 9-10, Dallas, TX, USA, 2015.

[13] J. E. F. Williams and D. L. Hawkings, "Sound generation by turbulence and Surfaces in arbitrary motion," *Philosophical Transactions of the Royal Society A: Mathematical, Physical and Engineering Sciences*, vol. 264, no. 1151, pp. 321–342, 1969.

[14] S. D'Angelo, F. Berardi, and E. Minisci, "Aerodynamic performances of propellers with parametric considerations on the optimal design," *The Aeronautical Journal*, vol. 106, no. 1060, pp. 313–320, 2002.

[15] S. Xiang, J. Wang, L. G. Zhang, S. X. Tong, J. Wu, and Y. Q. Liu, "A high efficiency propeller design method," *Journal of Aerospace Power*, vol. 30, no. 1, pp. 136–141, 2015.

[16] J. P. Yin and Z. W. Hu, "Effect of ground reflection and attenuation on the spectrum of sound source," *Journal of Nanjing University of Aeronautics and Astronautics*, vol. 03, pp. 22–28, 1990.

[17] SAE ARP 1846A, *Measurement of Far Field Noise from Gas Turbine Engines During Static Operation*, Society of Automotive Engineers International, 1990.

[18] Z. W. Yu and Y. H. Cao, "Numerical simulation of three-dimensional turbulent flow field of forward flying rotor," *Journal of Beijing University of Aeronautics and Astronautics*, vol. 32, no. 7, pp. 751–755, 2006.

[19] X. Ye, *Research on Helicopter Rotor Field and Noise Based on Unstructured Grid*, Master thesis of Nanjing University of Aeronautics and Astronautics, 2009.

[20] Z. Zhao, *Research on Wind Tunnel Experimental Technology of Propeller Characteristics*, Northwestern Polytechnical University, 2007.

[21] M. D. Moorel and B. Fredericks, "Misconceptions of electric propulsion aircraft and their emergent aviation markets," in *52nd AIAA Aerospace Sciences Meeting*, pp. 5077–5093, Reston, VA, USA, 2014.

[22] G. Snorri, *General Aviation Aircraft Design*, Elsevier, Oxford, UK, 2014.

[23] F. Farassat and G. P. Succi, "The prediction of helicopter rotor discrete frequency noise," *Vertica*, vol. 7, no. 4, pp. 309–320, 1983.

[24] F. Farassat, "Derivation of formulations 1 and 1A of Farassat," 2007, NASA-TM-2007-214853.